OXA β-lactamases from *Acinetobacter* spp. are membrane-bound and secreted into outer membrane vesicles

Lucia Capodimonte[1,2], Fernando Teixeira Pinto Meireles[3], Guillermo Bahr[1,2*], Robert A. Bonomo[4-7], Matteo Dal Peraro[3], Carolina López[1#] and Alejandro J. Vila[1,2,7#]

[1] Instituto de Biología Molecular y Celular de Rosario (CONICET IBR -UNR)

[2] Área Biofísica, Facultad de Ciencias Bioquímicas y Farmacéuticas, Universidad Nacional de Rosario, Rosario, Santa Fe, Argentina

[3] Institute of Bioengineering, School of Life Science, École Polytechnique Fédérale de Lausanne (EPFL), 1015 Lausanne, Switzerland.

[4] Department of Molecular Biology and Microbiology, Case Western Reserve University School of Medicine, Cleveland, Ohio, USA.

[5] Research Service, Louis Stokes Cleveland Department of Veterans Affairs Medical Center, Cleveland, Ohio, USA.

[6] Departments of Pharmacology, Biochemistry, Proteomics and Bioinformatics, Case Western Reserve University School of Medicine, Cleveland, Ohio, USA

[7] CWRU-Cleveland VAMC Center for Antimicrobial Resistance and Epidemiology (Case VA CARES), Cleveland, Ohio, USA.

Running title: Bla OXAs: Membrane Anchoring and Vesicle Secretion

Word count abstract: 246 words

Word count for the text: 4243

[#] Address correspondence to: Carolina López (lopez@ibr-conicet.gov.ar) and Alejandro J. Vila (vila@ibr-conicet.gov.ar). The author order was agreed by both authors based on seniority.

* Current address: Terragene, Ruta Nacional 9, Km 280, Parque Industrial Micropi 2130 Alvear, Argentina

ABSTRACT

β-lactamases from Gram-negative bacteria are generally regarded as soluble, periplasmic enzymes. NDMs have been exceptionally characterized as lipoproteins anchored to the outer membrane. A bioinformatics study on all sequenced β-lactamases was performed that revealed a predominance of putative lipidated enzymes in the class D OXAs. Namely, 60% of the OXA class D enzymes contain a lipobox sequence in their signal peptide, that is expected to trigger lipidation and membrane anchoring. This contrasts with β-lactamases from other classes, which are predicted to be mostly soluble proteins. Almost all (> 99%) putative lipidated OXAs are present in *Acinetobacter* spp. Importantly, we further demonstrate that OXA-23 and OXA-24/40 are lipidated, membrane-bound proteins in *Acinetobacter baumannii*. In contrast, OXA-48 (commonly produced by Enterobacterales) lacks a lipobox and is a soluble protein. Outer membrane vesicles (OMVs) from *Acinetobacter baumannii* cells expressing OXA-23 and OXA-24/40 contain these enzymes in their active form. Moreover, OXA-loaded OMVs were able to protect *A. baumannii, Escherichia coli* and *Pseudomonas aeruginosa* cells susceptible to piperacillin and imipenem. These results permit us to conclude that membrane binding is a bacterial host-specific phenomenon in OXA enzymes. These findings reveal that membrane-bound β-lactamases are more common than expected and support the hypothesis that OMVs loaded with lipidated β-lactamases are vehicles for antimicrobial resistance and its dissemination. This advantage could be crucial in polymicrobial infections, in which *Acinetobacter spp.* are usually involved, and underscore the relevance of identifying the cellular localization of lactamases to better understand their physiology and target them.

IMPORTANCE

β-lactamases represent the main mechanism of antimicrobial resistance in Gram-negative pathogens. Their catalytic function (cleaving β-lactam antibiotics) occurs in the bacterial periplasm, where they are commonly reported as soluble proteins. A bioinformatic analysis reveals a significant number of putative lipidated β-lactamases, expected to be attached to the outer bacterial membrane. Notably, 60% of class D OXA β-lactamases (all from *Acinetobacter* spp) are predicted as membrane-anchored proteins. We demonstrate that two clinically relevant carbapenemases, OXA-23 and OXA-24/40 are membrane-bound proteins in *A. baumannii*. This cellular localization favors secretion of these enzymes into outer membrane vesicles that transport them outside the boundaries of the cell. β-lactamase-loaded vesicles can protect populations of antibiotic-susceptible bacteria, enabling them to thrive in the presence of β-lactam antibiotics. The ubiquity of this phenomenon suggests that it may have influenced the dissemination of resistance mediated by *Acinetobacter* spp., particularly in polymicrobial infections, being a potent evolutionary advantage.

KEY WORDS: lipidated β-lactamases, OXA β-lactamases, *Acinetobacter* spp., outer membrane vesicles, dissemination of antimicrobial resistance

INTRODUCTION

Bacteria possess a potent and diverse arsenal to resist the action of antibiotics. Gram-negative bacteria have predominantly evolved the expression of β-lactamases as one of the main mechanism of resistance against β-lactam antibiotics (1, 2). To date, more than 8200 different β-lactamase variants are reported (3), a number that is increasing at an alarming pace. The evolution and dissemination of genes coding for β-lactamases in opportunistic and pathogenic bacteria has been accelerated by the misuse and overuse of antibiotics worldwide, representing a major challenge for public health (1, 4).

β-lactamases are classified into four groups (A, B, C and D) according to the Ambler system, based on sequence homology (5). Class A, C and D enzymes are serine-β-lactamases (SBLs), which share a common protein fold, but display differences in their active sites and catalytic mechanisms (6, 7). In contrast, class B enzymes are metallo-β-lactamases (MBLs) requiring Zn(6) ions for their hydrolytic activity (8). From the clinical point of view, carbapenemases are the largest public health threat since they are able to inactivate carbapenems, the most potent β-lactams available in clinical practice (9, 10). Carbapenemases have been identified three out of these four classes, including all class B MBLs, members of class A (KPC, GES and NMC) and many class D β-lactamases (from the OXA family, named upon their oxacillinase activity) (11, 12).

In Gram-negative bacteria, mature β-lactamase enzymes are localized in the periplasmic space (13-16), where they cleave β-lactam antibiotics, thwarting their activity against enzymes involved in peptidoglycan cross-linking. β-lactamases have been historically regarded as soluble periplasmic enzymes. In contrast, a reduced number of β-lactamases have been exceptionally characterized as lipoproteins anchored to the inner leaflet of the outer membrane, such as the class A enzymes BRO-1 from *Moraxella catarrhalis* (17) and PenI from *Burkholderia pseudomallei* (18). More recently, the widespread Zn-dependent carbapenemase NDM (6) (with 68

reported clinical variants to date) was identified as a lipidated, membrane-bound enzyme, a localization that enhances the stability of this enzyme upon the zinc starvation process during an infection (19, 20).

β-lactamases are produced as cytoplasmic precursors with an N-terminal signal sequence (the signal peptide) that directs these precursors to one of the two main export pathways (Sec or Tat) responsible for protein translocation into the periplasmic space (13). Most biochemically characterized β-lactamases have been shown to translocate across the inner membrane via the Sec system (14, 16). In the case of soluble, non-lipidated β-lactamases, the type I signal peptidase (S cleaves the signal peptides of the precursor enzymes to generate the mature proteins (13, 21, 22). Instead, in the case of lipoproteins, the signal peptides are cleaved by the type II signal peptidase (SpII) during the lipoprotein maturation process (16, 22). Lipoprotein precursors possess a characteristic 4 amino acid motif known as a lipobox (23). The lipobox consensus sequence is [LVI]-[ASTVI]-[GAS]-C (24-26). The lipidation machinery in the periplasm transfers a diacylglycerol group to the free sulfhydryl of the cysteine residue in the lipobox and cleaves the signal sequence, leaving an acylated cysteine at the N-terminus. A further acyl group is then added generating a mature, triacylated lipoprotein that is inserted into the membrane (27). This lipidation mechanism has been thoroughly characterized in *E. coli* and it is widespread among Enterobacterales and non-fermenters (25, 28, 29).

In the case of NDM-1, membrane anchoring stabilizes this MBL against zinc deprivation and favors its incorporation into outer membrane vesicles (OMVs) (19). These nano-sized spherical structures bud and detach from the outer membrane of Gram-negative bacteria (30), playing several roles as decoys for phages and antibiotics, transporting nucleic acid, outer membrane and periplasmic proteins as well as insoluble cargo (31, 32). Similar processes have been also reported in Gram-positive organisms (33). NDM incorporation into vesicles increases the available enzyme levels at the infection site, extending antibiotic hydrolysis beyond the limits of

the bacterial cell (20). As a result, NDM-loaded vesicles can protect populations of otherwise antibiotic-susceptible bacteria (19). Furthermore, vesicles can also mediate the transfer of the *bla*$_{NDM-1}$ gene between bacteria (34, 35). The selection of the protein cargo in the case of NDM-1 depends on the interaction with the bacterial membrane, in which the covalent attachment through the lipid moiety is the main determinant (36, 37).

To explore the ubiquity of lipidation among β-lactamases, we performed a bioinformatic analysis of the signal peptides of all β-lactamases deposited in the β-lactamase database (www.BLDB.eu) (3). This study reveals a low number of lipobox sequences in enzymes from classes A, B, and C. In contrast, almost 60% of class D β-lactamases (all of them OXA enzymes) have a lipobox sequence and are thus predicted to be membrane-bound lipoproteins. Noteworthy, all putative OXA β-lactamase lipoproteins are found in *Acinetobacter* spp. Herein, we provide experimental evidence that the clinically relevant carbapenemases OXA-23 and OXA-24/40 from *A. baumannii* are membrane-bound lipoproteins. Disruption of the lipobox via mutagenesis results in the expression of soluble enzymes, supporting the bioinformatics analysis and molecular simulations.

The membrane-bound localization of OXA β-lactamases favors their incorporation into OMVs, as reported for NDM-1. The evolving hypothesis is that these OXA-loaded vesicles are capable of improving survival of not only *Acinetobacter* spp. in conditions of high β-lactam concentrations but also β-lactam-susceptible bacteria that are present in polymicrobial infections. We conclude that membrane-bound β-lactamases and their vesicle packaging represent a significant adaptation response in *Acinetobacter* spp. We propose that this cellular localization, linked to the secretion of lactamases into OMVs, represents an evolutionary advantage for *A. baumannii*, a highly troublesome pathogen associated with community-acquired and nosocomial infections. The protective effect of these vesicles confers a population advantage provided by *A. baumannii* OXA-producers in multiple clinical environments.

159

RESULTS

Bioinformatics predict that most class D β-lactamases (OXAs) are lipidated

To identify putative lipidated β-lactamases, we performed an *in silico* analysis of all β-lactamase sequences available in the BLDB database (3) using the SignalP 6.0 server (38). This server employs a machine-learning algorithm that classifies signal peptides into one of the five known types (Sec/SPI, Sec/SPII, Sec/SPIII, Tat/SPI and Tat/SPII) by means of a score that predicts the possibility of the signal peptide being transported and processed by each system. Our intention was to label all reported β-lactamases into soluble and lipidated enzymes. Despite the focus of the current work being on β-lactamases in Gram-negative organisms, the analysis covered all sequenced enzymes.

From a total number of 7479 accessible β-lactamase sequences (April 2024), 7226 were predicted to contain an N-terminal signal peptide targeting the Sec translocation pathway (97 %) (Fig. 1A), confirming that most β-lactamases are Sec substrates (16). The small proportion of β-lactamases predicted to be translocated by the Tat system mostly belong to highly divergent class A enzymes, suggesting that this feature does not imply any evolutionary connection among them but, instead, an adaptation to each organism. Indeed, there are enzymes from Gram-negative bacteria such as *Burkholderia* spp. (PenA and PenI enzymes), *Xanthomonas* spp. (XCC enzymes) and *Mycobacterium* spp. (MFO from M. fortuitum and MAB from *M. abscessus*) and from the Gram-positive organism *Streptomyces* spp. (SDA enzymes) (Supplementary Table 1).

The identification of a lipobox sequence helps annotate proteins as substrates of the signal peptidase II, therefore targets for lipidation and membrane anchoring. Lipoboxes were identified in the sequences of 17% of class A enzymes, 10 % of class B, and only two (0.3%) class C β-lactamases (Fig. 1B and Table 1). This result agrees with the consensus that considers β-lactamases as soluble periplasmic proteins. In stark contrast, ca. 60% of class D enzymes are putative lipoproteins (Fig.1B and Table

2). Table 1 shows several representative class A and B β-lactamases predicted as lipidated proteins, while Table 2 lists all families of putative lipidated OXAs. We also indicate the most likely translocation and processing pathway in each case. Supplementary Table 1 includes the predictions for all β-lactamases, with the scores provided by the SignalP 6.0 server.

The putative lipoproteins belonging to class A include an important number of enzymes from Gram-positive and Gram-negative bacteria, a few of them already characterized experimentally. BcIII from *Bacillus cereus* was the first characterized membrane-bound lactamase (39). Later, BRO-1 was the first β-lactamase from a Gram-negative bacteria characterized as a membrane-bound protein (17). BRO-1 and BRO-2 from *Moraxella catarrhalis*, are both predicted as lipoproteins dependent on the Tat system. PenI enzyme from *B. pseudomallei* was experimentally shown to be a membrane-bound protein (18). Here we show that the variants of PenA, PenB, PenI and other members of the Pen family produced by *Burkholderia* species are predicted as lipoproteins translocated by the Tat system.

In the case of class B MBLs, subclass B1 includes all variants of AFM and NDM enzymes, CHM-1, and ZOG-1, as putative lipoproteins dependent on the Sec system. No proteins from subclass B2 were predicted to be lipidated with a high score. However, within subclass B3, certain enzymes were identified as lipoproteins (Table 1).

Most class D β-lactamases are also known as oxacillinase enzymes or OXAs (12). Remarkably, all putative lipidated OXAs are chromosomally-encoded or acquired from *Acinetobacter* species, except for OXA-63-like enzymes from *Brachyspira pilosicoli*, OXA-347, -1089 and -1090 (26 out of 735 OXA enzymes). Indeed, the main groups of carbapenem-hydrolyzing class D β-lactamases (CHDL) were predicted as lipoproteins: the chromosomally-encoded OXA-51-like and the acquired OXA-23-like, OXA-58-like and OXA-24/40-like (Table 2). In contrast, soluble OXA enzymes are not predicted in *Acinetobacter* species. This direct link between protein lipidation and a bacterial host (*Acinetobacter*, in this case) is unique to class D enzymes, since

lipidated class A and B enzymes are found in a wide variety of bacterial hosts (Table 1 and Table 2).

Molecular simulations reveal a mechanism for membrane association for lipidated OXA β-lactamases

To better characterize their possible association with membranes, we selected and performed coarse-grained molecular dynamics (CG-MD) simulations of the two most clinically important β-lactamases related to carbapenem resistance: OXA-23 and OXA-24/40. We ran the simulations with a lipid bilayer mimicking the composition of the inner leaflet of the *A. baumannii* outer membrane (12% cardiolipin, 16% phosphatidylglycerol (PG), and 72% phosphatidylethanolamine (PE) (see Methods)). The enzymes were triacylated at their N-terminal cysteine residue, as suggested by the bioinformatic analysis of the signal peptide. In all simulations (5 MD replicas) both enzymes readily anchored into and kept attached to the lipid bilayer via the triacyl moiety in their N-terminus. OXA-23 and OXA-24/40 adopted similar orientations on the membrane, laying their globular domain on its surface while leaving their active site facing the periplasmic space (Supplementary Movies 1 and 2; Fig. 2).

This positioning of OXA-23 and OXA-24/40 might be a structural feature that prevents the occlusion of their active-site by interaction with the lipid bilayer, as the same phenomenon has been observed in MD studies of lipidated NDM-1 (36).

Cardiolipin molecules displayed considerably high contact frequency (percentage of the simulation time) with the globular domain of OXA-24/40, despite representing only 12% of the membrane's lipid composition, notably with residues Arg151 (56.9%), Arg190 (53.8%), Lys61 (53.2%), Lys150 (45%), and Lys147(43.3%) (Fig 2B). Albeit to a lesser extent, the residues in the analogous positions in OXA-23 also helped stabilize the enzyme's conformation on the membrane surface via cardiolipin interactions as measured by contact frequency: Arg149 (26.9%), Lys148 (25%), Lys145 (21.9%), and Lys60 (20.1%) (Fig 2B). Despite not being essential for membrane anchoring, these

electrostatic interactions could help orient OXA-23 and OXA-24/40 in such a way that their active-sites remain available to substrate binding.

OXA-23 and OXA-24/40 are lipidated, membrane anchored proteins

To experimentally test the bioinformatic predictions and the molecular simulations, we performed cellular fractionation experiments. We selected the two putative lipidated OXA-23 and OXA-24/40 expressed in *A. baumannii* , and a putative soluble periplasmic OXA, OXA-48, lacking a lipobox sequence and commonly produced by Enterobacterales such as *K. pneumoniae* and *E. coli* (Fig. 3A) (12). All these selected proteins are clinically relevant carbapenemases (1, 9).

These three proteins were expressed by the pMBLe_OA plasmid with their native signal peptides and with a Strep-tag (ST) fused to the C-terminal to allow uniform immunodetection (37). We chose *A. baumannii* ATCC 17978 and *Escherichia coli* ATCC 25922 as laboratory strains for the different organisms with isogenic backgrounds. The grown cells were subjected to a cell fractionation assay, which allowed collecting the periplasmic fraction (Per) after treatment with lysozyme. Sonication then led to the separation of total membranes (40) from the cytoplasm (Cyt). Whole cells (WC) and each fraction were analyzed by immunoblotting with anti-ST antibodies for the β-lactamases. Specific antibodies against cytoplasmic RNA polymerase (RNApol) and the outer membrane protein A (OmpA), were used as controls for the quality of the preparation of the soluble and membrane fractions, respectively. Fig. 3B shows that OXA-23 and OXA-24/40 were present in the membrane fractions of *A. baumannii*, with no accumulation of these proteins in the periplasmic fraction. In contrast, OXA-48 was detected only in the periplasmic fraction of *E. coli* as a soluble β-lactamase (Fig. 3B).

The lipobox is a signature sequence of bacterial lipoproteins, and the cysteine residue located at its C-terminus is the target of lipidation. To confirm the role of this residue in the localization in the membrane fraction of OXA 23 and OXA-24/40 in *A.*

baumannii, we substituted the Cys for Ala in both proteins (Cys18 in OXA-23 and Cys20 in OXA-24/40) (Fig. 3A) and analyzed the impact of this replacement in the cellular localization of both enzymes. Expression of the Cys18Ala_OXA-23 (CA_OXA-23) and Cys20Ala_OXA-24/40 (CA_OXA-24/40) variants in *A. baumannii* resulted in the accumulation of both proteins only in the periplasmic fractions as soluble proteins, separately from OmpA, which is present in total membrane fractions, confirming our hypothesis (Fig. 3C).

To assess the nature of the interaction between the bacterial membrane and OXA-23 and OXA-24/40, we attempted to solubilize these enzymes from the pure *A. baumannii* membranes using different methods. Treatment with high ionic strength (1 M NaCl) and highly basic pH (0.1 M Na_2CO_3 pH 11.5) did not release any of the two OXAs from the membrane fractions (Fig. 3D), indicating that they are not peripheral proteins associated with the membrane by only means of electrostatic interactions, although these interactions can better expose the active side to the periplasmic space, as observed with MD simulations (Fig. 2). Instead, OXA-23 and OXA-24/40 were only solubilized upon treatment with 1% w/v Triton X-100 (Fig. 3D), confirming that both enzymes interact with the membrane through hydrophobic interactions. Overall, these results establish that OXA-23 and OXA-24/40 are lipidated, membrane-bound proteins in *A. baumannii*.

The MIC values of piperacillin and imipenem against *A. baumannii* cells expressing the soluble and membrane-bound variants of both OXA-23 and OXA-24/40 were similar (Suppl. Table 3), revealing that the cell localization does not contribute to the resistance phenotype.

Lipidated OXAs are selectively secreted into OMVs

We then explored whether membrane anchoring of OXAs results in packaging into OMVs. We purified OMVs from *A. baumannii* expressing native OXA-23 and OXA-24/40, and the soluble variants CA_OXA-23 and CA_OXA-24/40 and quantified the

protein levels in the vesicles. Despite the protein levels of lipidated and soluble variants were comparable in whole cells, only the lipidated OXAs were incorporated at high levels in OMVs from *A. baumannii* (Fig. 4A). Fig. 4B shows that removal of the lipidation site for CA_OXA-23 leads to a substantial decrease of approximately 95% in the transported enzyme by vesicles. Similarly, in the case of CA_OXA-24/40, there is an approximately 85% reduction in the level of the enzyme into OMVs, indicating that membrane anchoring contributes to the selective secretion of OXA-23 and OXA-24/40 in *A. baumannii* cells.

To assess whether the OXA enzymes are located in the lumen of the vesicles or pointing outwards, we exposed the OXA-loaded vesicles to proteinase K to assess the accessibility of this protease to the enzymes in the OMVs. Treatment of the intact vesicles with proteinase K did not alter the levels of OXA-23 or OXA-24/40. Instead, both enzymes were completely degraded by proteinase K in Triton-lysed vesicles (Fig. 4C). These experiments suggest that the proteins are located in the lumen of the OMVs, confirming the protective role of the vesicles from extracellular degradation when these enzymes are secreted.

OXA-loaded OMVs protect β-lactam-susceptible bacteria

We then attempted to determine if the OXAs incorporated into vesicles were in their active forms by examining the protective effect of β-lactamase-loaded vesicles in β-lactam-susceptible bacteria. We tested this in β-lactam-susceptible *A. baumannii, E. coli,* and *P. aeruginosa* cells treated with OMVs from *A. baumannii* carrying the empty vector (EV) or expressing OXAs in the presence of imipenem or piperacillin, and we determined the MICs.

Incubation of β-lactam-susceptible *A. baumannii* with OMVs loaded with lipidated OXA-24/40 resulted in a MIC against imipenem of 32 μg/ml versus a MIC of 2 μg/ml for those cells incubated with vesicles loaded with the soluble variant, and a MIC

of 0.125 μg/ml for control vesicles isolated from *A. baumannii* cells transformed with the empty plasmid (Fig. 5A and Supplementary Table 4). The same trend was observed for β-lactam-susceptible *E. coli* and *P. aeruginosa* cells and for OXA-23 and its soluble variant. In this case, the β-lactam-susceptible *A. baumannii* cells grew at 8 μg/ml imipenem when incubated with OXA-23-containing OMVs versus 1 μg/ml imipenem for vesicles loaded with the soluble variant CA_OXA-23 (Fig. 5A and Supplementary Table 4). A similar protection effect was observed for piperacillin, with a high impact in the MICs for the three tested β-lactam-susceptible bacteria when were incubated with OMVs loaded with lipidated OXAs (Fig. 5B and Supplementary Table 4). The trend of enhanced protection with a higher MIC when using OXA-24/40-loaded vesicles compared to OXA-23-loaded vesicles is likely attributed to the higher levels of OXA-24/40 in the concentration of OMVs used during the incubation experiment with susceptible bacteria. In fact, the levels of OXA-24/40 in the OMVs were approximately four times higher than those of OXA-23. Overall, these results indicate that OXA enzymes are active within vesicles produced by *A. baumannii,* playing a collective role improving the viability of antibiotic-susceptible bacteria and that this role is highly dependent on the membrane localization of these enzymes.

DISCUSSION

Antimicrobial resistance (AMR) is an inevitable consequence of the use of antibiotics. β-lactamases represent the predominant mechanism of resistance to β-lactam antibiotics, as accounted by the early report of a penicillinase in 1940 before the clinical use of antibiotics (41). In the current century, we have witnessed an alarming spread of resistance genes coding for β-lactamases among pathogenic and opportunistic bacteria, with > 8,000 variants reported so far. Biochemistry and structural studies have described the mechanistic and structural features eliciting resistance to new drugs (42). However, there are still many aspects incompletely understood about the biochemical and mechanistic aspects of β-lactamases. Indeed, the catalytic mechanism of metallo-β-lactamases was dissected only 5 years ago(43), and a recent paper disclosed the role of anions in the biphasic nature of the kinetics of OXA enzymes(44, 45).

In addition to these biochemical issues, host-specific aspects of β-lactamases are poorly understood. For example, it is not clear why some enzymes, despite being plasmid-borne, are confined to some bacterial host(s), while others are present in a wider variety of microorganisms. This phenomenon has been recently addressed in the case of metallo-β-lactamases (46), but it is not defined for serine-dependent enzymes. Finally, the bacterial physiology of β-lactamases in the periplasm of Gram-negative bacteria is scarcely characterized, a problem that includes the incomplete knowledge of the cellular localization of these enzymes, which can be soluble or membrane-bound. The latter was shown to be the case of NDM-1 and its different allelic variants (47). The cellular localization of NDM variants improves the stability of these enzymes and favors their incorporation into OMVs from different bacteria (19, 46).

The identification of a lipobox sequence helps annotate a protein as putative lipidated and membrane-bound. In this work we examined the distribution of lipoboxes in the signal peptides of β-lactamases from all 4 classes. We found that the distribution

of putative lipidated enzymes is diverse, depending on the class of β-lactamase and the microorganism. Within the class A group, representing one fourth of reported β-lactamases, only 15% of enzymes contain lipoboxes. Two of them, BRO from *Moraxella catarrhalis* and PenI from *B. pseudomallei*, have already been characterized biochemically. Within class B, all NDM variants are membrane-bound (68 out of > 800 enzymes), which have been reported in Enterobacterales and non-fermenters. Instead, class D enzymes are singular since 60% of the OXA β-lactamases contain a lipobox, all of them (with only one exception) being expressed in *Acinetobacter* spp. This suggests a host-specific effect for these enzymes that contrast with the host distribution of lipidated class A and class B β-lactamases.

Coarse-grained MD simulations predict that the lipid moiety attached to a Cys residue in the lipobox of OXA-23 and OXA-24/40 is inserted in the lipid bilayer in such a way that a patch in the globular domains of these enzymes presents an attractive interaction with the bacterial membrane. This interaction is expected to favor and stabilize membrane binding as well as to orient the enzyme active site towards the periplasm.

We validated these predictions by cellular fractionation and immunoblotting experiments, that reveal that OXA-23 and OXA-24/40 are lipidated, membrane-bound proteins in *Acinetobacter* spp. Mutagenesis of the Cys residue in the lipobox gives rise to soluble proteins in both cases. We also studied as a control OXA-48 (lacking a lipobox), a soluble, periplasmic enzyme in *E. coli*.

Both OXA-23 and OXA-24/40 were secreted into OMVs from *A. baumannii*. In both cases, the soluble variants resulting from a mutation at the lipobox were also secreted into OMVs, but to a much smaller content. This behavior is similar to what has been reported for NDM, i.e., membrane anchoring significantly facilitates secretion into vesicles, but the soluble variants can also be secreted (19). Incubation of different antibiotic-susceptible bacteria with OXA-loaded OMVs resulted in a protective effect of these bacteria against a carbapenem and a penicillin. In all cases, the protective effect

(measured as an increase in the MIC) correlates with the amount of protein present in the OMVs. This reveals that both OXA-23 and OXA-24/40 are secreted in their active form, as is the case for NDM-1.

The current results help unify many findings in the literature and coalesce different observations. OXA-23 has been shown to display an extensive interaction network in *A. baumannii* by cross-linking and mass spectrometry experiments (48). OXA-23 interacts with the outer membrane proteins OmpA, OmpW, CarO and ABUW_2898, as well as with YiaD, an outer membrane protein that has been related to carbapenem resistance. In all these cases, the cross-linking was observed through residue Lys60 in OXA-23, which is one of the positively charged residues in the protein surface identified as making transient interactions with the outer membrane (Fig. 2). We propose that the reported interaction (48) is due to the proximity of OXA-23 to the outer membrane.

A proteomics analysis of OMVs from the multi-drug resistant clinical isolate *A. baumannii* DU202 revealed that OXA-23 accounted for 36% of the total protein content in OMVs (49). Thus, despite the relatively low levels of expression of OXA-23 in the current model organism, secretion of OXA β-lactamases into OMVs in clinical strains can be a relevant phenomenon. Liao and coworkers (50) informed the finding of OXA-58 in the lumen of OMVs from *A. baumannii* Ab290. Our analysis (Table 2) predicts the OXA-58 family as lipidated, also supporting this finding.

OMVs have been suggested to play different roles in bacteria. These vesicles are essential in cellular detoxification processes, by removing toxic periplasmic components that elicit envelope stress and compromise bacterial fitness. This has been shown to be the case for some class B β-lactamases when expressed in non-frequent bacterial hosts, such as VIM-2 and SPM-1 (46). Colquhoun *et al*. recently observed that hyperexpression of OXA-23 in *A. baumannii* induces collateral physiological damages by altering the peptidoglycan integrity (51). We postulate that the incorporation of OXA-23 into OMVs might mitigate the negative impact of OXA-23

overexpression by reducing the effective concentration of OXA-23 in the periplasm, at the same time increasing the levels of this β-lactamase in the environment by its presence in OMVs, thus contributing to resistance.

We also show here that OXA-loaded vesicles are able to protect bacterial populations of otherwise susceptible *A. baumannii*, *P. aeruginosa* and *E. coli* from the activity of β-lactam antibiotics. Therefore, the expression of lipidated OXA enzymes may provide an advantage both for the producing organism and in polymicrobial infections. Indeed, multi-drug resistant *Acinetobacter* spp. is increasingly reported in co-colonization events in intensive care units with Enterobacterales expressing extended spectrum β-lactamases (ESBLs) (52-54). A recent analysis from Semenec and coworkers (55) has described the relevance of cross-protection of *A. baumannii* on *K. pneumoniae* against cefotaxime in a polymicrobial lung infection. In addition, this protein-mediated protection effect could be coupled to plasmid transfer. The seminal work from Bou and coworkers reported the role of OMVs in transferring the plasmid containing the $bla_{\text{OXA-24/40}}$ gene between different *A. baumannii* strains (56). Overall, this calls for a deeper understanding of the role of OMVs in polymicrobial infections through studies able to assess the biochemical bases of cross-protection, including the presence of different β-lactamases as selective vesicle cargo.

In closing, this work also underscores the relevance of studying the physiology of β-lactamases in their native bacterial hosts when using model organisms with isogenic backgrounds. The identification of a large, clinically relevant family of β-lactamases as membrane-bound proteins in *A. baumannii* linked to their presence in vesicles requires us to address novel approaches to clinical treatments, particularly in polymicrobial infections.

MATERIALS AND METHODS

Bioinformatic analysis

The Entrez module from the Biopython library (56) was used to access the FASTA sequences from the NCBI database using the accession codes listed in the "GenPeptID" column of the β-lactamase database (3). The ignore list command was utilized to exclude entries containing dashes, blank spaces, “assigned”, and “Withdrawn”. For enzymes with multiple accession numbers, the first one listed was selected. All sequences were compiled into a list, which was then saved as a text file. The Python script is available upon request. The generated file was used as the input for the SignalP 6.0 server available at https://services.healthtech.dtu.dk/services/SignalP-6.0. The prediction was executed in slow mode, with "short output" and "Other" selected as the organism option. The results were downloaded as a JSON summary, copied into Supplementary Table 1, and aligned with the information from the β-lactamase database.

CG-MD simulations

Structures of OXA-23 and OXA-24/40 were obtained from the AlphaFold Protein Structure Database (AFDB) (58) under the UniProt accession codes A0A068J749 and Q8RLA6, respectively (59). This was done as the structures of these enzymes deposited in the Protein Data Bank (PDB) (60) lacked a considerable portion of both proteins N-terminal sequence, including the cysteine residue that is lipidated. Nonetheless, the globular domains of both enzymes’ models were inspected and compared to their deposited structures, confirming that the models had excellent accuracy (OXA-23 AF model pLDDT = 95.7, RMSD against PDB ID 4JF4 = 0.427 Å; OXA-24/40 AF model pLDDT = 95.7, RMSD with PDB ID 3ZNT = 0.208 Å). The models in the AFDB are computed based on the proteins’ complete sequence, so it was necessary to remove the signal peptides of both OXA-23 (up to Cys18) and OXA-24/40 (up to Cys20).

The simulations were performed using the MARTINI 3.0 forcefield (40). The first step involved the coarse-graining of the protein models done using the Martinize 2 tool (61). An elastic network with a bond force constant of 500 kJ mol^{-1} nm^{-2} and lower and upper elastic bond cut-offs of 0.5 and 0.9 nm, respectively, were implemented to stabilize the tertiary structure of the proteins. The parameters and structure of the triacyl moiety covalently attached to the N-terminus cysteine were taken from Rao et al. (62), who also made available a Python script to generate an initial configuration for the lipidated residue. The INSert membrANE (*insane*) program (63) was used to build the simulation systems: a tetragonal box of dimensions 13x13x15 nm^3 (X, Y, Z) containing a symmetric lipid bilayer of 72% POPE, 16% POPG, and 12 % cardiolipin, mimicking the composition of the *A*. *baumannii* OM inner leaflet (64). The systems were immersed in water with either OXA-23 or OXA-24/40 positioned 7 nm away from the membrane surface. The parameters for cardiolipin were obtained from Corey et al. (65), while the others lipids were already included in the official release of the MARTINI 3.0 force field. The systems were then neutralized with Na^+ counter ions.

GROMACS (66) version 2022.1 was used to run all the MD simulations. In all stages of the procedure, the cut-off radius for short-range electrostatic and van der Waals interactions was 11 Å; The reaction field method (67) was implemented to calculate long-range electrostatic interactions. Periodic boundary conditions were applied in all directions. Energy minimization and equilibration of the systems was performed as per the recommended protocol of the CHARMM-GUI web server (68) as of July 2023. The production dynamics were performed in the NPT ensemble, with the V-rescale thermostat (69) and the Parrinello-Rahman barostat (70). Both systems had five replicas and each ran for 4 µs. Protein-lipid interaction analyses were performed with the ProLint Web Server (71), using an interaction cut-off of 6 Å. The Visual Molecular Dynamics (VMD) (72) software was used for visual inspection of the simulations and recording of the movies. All protein and membrane images were generated with ChimeraX (73).

509

510 **Bacterial strains, culture conditions and plasmid constructions**

511 *Escherichia coli* ATCC 25922 and *Acinetobacter baumannii* ATCC 17978 were
512 used for expression of the empty vector pMBLe-OA and also for expression of the
513 different OXAs. The *bla*$_{OXA}$ genes were cloned into the pMBLe-OA vector (46) fused to
514 a Strep-Tag II sequence and downstream of a pTac promoter inducible by isopropyl β-
515 d-1-thiogalactopyranoside (IPTG). All strains were grown aerobically at 37 °C in
516 lysogeny broth (LB) medium supplemented with gentamicin 20 µg/mL when necessary.
517 Expression of the enzymes were induced at OD = 0.4 by adding 10 µM IPTG and
518 incubated for 4 h at 37 °C.

519 Chemical reagents were purchased from Sigma-Aldrich.

520

521 **Variant constructions by PCR Overlap**

522 The soluble variants of OXA-23 and OXA-24/40 were constructed by site-
523 directed mutagenesis using overlapping primers. For each enzyme we amplified the full
524 length *bla*$_{OXA}$ genes, including their native signal peptides from a pUC57 (Macrogen®)
525 plasmid using mutagenic primers and internal plasmid primers called pMBLe_Fw 5'-
526 GCTGTTGACAATTAATCATCGGCTC-3' and pMBLe_Rv 5'-
527 CGTAGCGCCGATGGTAGTG-3'.

528 To construct CA_OXA-23 we used the following couple of primers: pMBLe_Fw
529 5'-AAATTATGCTGAACCGTAGCACCAGAAAGAAAAAG-3' and pMBLe_Rv 5´-
530 CTTTTTCTTTCTGGTGCTACGGTTCAGCATAATTT-3'.. The double stranded DNA
531 obtained and the plasmid pMBLe were cleaved using *Nde*I and *Eco*RI and therefore
532 ligated. Then, pMBLe-OXA-23 was digested with *Bam*HI and *Eco*RI and ligated with
533 pMBLe_OA digested with the same enzymes.

534 To construct CA_OXA-24/40, we used the following series of primers:
535 pMBLe_Fw 5'-AGTTTTAATAGATGAAGCTGCACTGAGAGAAACTAG-3´ and
536 pMBLe_Rv 5´-CTAGTTTCTCTCAGTGCAGCTTCATCTATTAAAACT-3' . The double

537 stranded DNA obtained and the plasmid pMBLe were cleaved using *Nde*I and *Hind*III
538 and were then ligated. Molecular biology enzymes were purchased from Thermo-
539 Fisher®, and primers were ordered from Invitrogen®.
540
541 **Cell fractionation**
542 The fractionation protocol was based in the one described by Pettiti et al (74).
543 The cells were pelleted and resuspended in 0.2 M Tris at pH 8, 1M sucrose, 1mM
544 EDTA in a proportion of 10 mL per initial culture liter. Lysozyme 1mg/mL was added
545 and incubated for 5 minutes at room temperature. The suspension was centrifuged
546 during 20 minutes at 30,000 x g, the supernatant content the periplasmic fraction and
547 the pellet the spheroplast and membrane remains. The pellet was resuspended in
548 10mM Tris at pH 8.5 EDTA 2.5 mM 10 µg/mL DNAse 1mM PMSF and sonicated. Once
549 cell debris were removed, the suspension was ultracentrifuged at 45,000 x g for 45
550 minutes. The supernatant containing the cytoplasm was collected. The pelleted total
551 membrane was resuspended in 10 mM Hepes, 0.2 M NaCl at pH 7.5. The
552 resuspension volumes were normalized according to the OD_{600} and the initial culture
553 volume.
554
555 **Selective membrane protein solubilization**
556 Membrane proteins were extracted sequentially. Firstly, the total membrane
557 fraction was pelleted by ultracentrifugation at 45,000 x g during 45 min and gently
558 resuspended in cold 1 M KCl. After 30 min incubation on ice they were ultracentrifuged
559 again. The supernatants containing loosely associated peripheral proteins were
560 collected and the pellets were resuspended in 0.1 M Na_2HCO_3 at pH 11.5. After a
561 30min incubation on ice to release peripheral proteins associated by strong
562 electrostatic interactions were centrifugated again. The pellets were resuspended in
563 1% w/v Triton X-100 and incubated 30 min on ice to extract integral or hydrophobically-

564 associated proteins in detergent micelles. The supernatants were collected, and the
565 pellets were resuspended in 10 mM Hepes, 0.2 M NaCl at pH 7.5.
566
567 **Protein Immunodetection**
568 Immunoblotting assays were realized in PVDF membranes using Strep-Tag® II
569 monoclonal antibodies (at 1:1000 dilution from a 200 µg/ml solution) (Novagen®) and
570 immunoglobulin G-alkaline phosphatase conjugates (at 1:5000 dilution). Monoclonal
571 anti-RNApol was used as a cytoplasmic control and polyclonal anti-OmpA kindly
572 provided by Dr. Alejandro Viale was used as a membrane marker.
573 The whole cells, periplasm and cytoplasm samples were normalized according
574 to the following equation: $V = 100\ \mu L \times OD_{600} \times V_c$, where V_c is the starting volume of
575 culture sample. Total membranes fraction and OMVs were normalized according to a
576 lipid quantification by FM4-64 (Thermofisher®). Protein band intensities were quantified
577 by using Gel Analyzer software (75).
578
579 **Purification of OMVs and OXAs levels detection into OMVs**
580 Overnight cultures of *A. baumannii* pMBLe-OA-*bla* cells were grown in 300 mL
581 of LB broth at 37°C, reaching an OD_{600} of 0.4. Subsequent induction with 20 µM IPTG
582 was followed by continued overnight growth with agitation. The cells were harvested,
583 and the supernatant was filtered through a 0.45-µM membrane (Millipore). Ammonium
584 sulfate was added to the filtrate at a concentration of 55% (w/vol), followed by overnight
585 incubation with stirring at 4 °C. Precipitated material was separated by centrifugation at
586 12,800 × g for 10 min, resuspended in 10 mM HEPES, 200 mM NaCl at pH 7.4, and
587 dialyzed overnight against >100 volumes of the same buffer. Next, samples were
588 filtered through a 0.45-µM membrane, layered over an equal volume of 35% (w/vol)
589 sucrose solution, and ultracentrifuged at 150,000 × g for 1 h and 4 °C. Pellets
590 containing the OMVs were washed once with 10 mM HEPES, 200 mM NaCl at pH 7.4,
591 and stored at −80 °C until use.

The OMVs were quantified by two different methods. The total protein concentration was measured by the Pierce bicinchoninic acid (BCA) protein assay kit (Thermo Scientific®) as described (37). Lipid content associated with OMVs was determined using the lipophilic fluorescent dye FM4-64 (Thermofisher®) as described previously (76). Briefly, a portion of OMVs was incubated with FM4-64 (2 µg/ml in PBS) for 10 min at room temperature. Separate samples of OMVs and the FM4-64 probe were used as negative controls. After excitation at 515 nm, emission at 640 nm was measured with the multiplate reader SYNERGY HT (Biotek®).

The OMV content was analyzed by SDS-PAGE and immunoblotting. Gel lanes were equally loaded based on total protein and lipid content. The pre-stained *Blue Plus® II* Protein Marker (14-120 kDa) provided molecular weight standards for Fig. 4. To determine the levels of OXA-23, CA_OXA-23, OXA-24/40, and CA_OXA-24/40 in OMVs, the mature protein band intensities in whole cells (WC) and in the OMVs, derived from *A. baumannii* expressing each OXA protein, were quantified from polyvinylidene difluoride (PVDF) membranes using GelAnalyzer software (53). The quantity of each OXA protein in the OMVs (from immunoblots) was divided by the quantity of each OXA in whole cells (from immunoblots). Finally, the values plotted in Fig. 4B (expressed as a percentage) correspond to the normalization of the levels of each soluble OXA (CA_OXA-23 or CA_OXA-24/40) to the value of its corresponding wild-type OXA (OXA-23 or OXA-24/40), which was taken as 100 percent.

Proteinase K accessibility assay

OMVs were resuspended in a buffer containing 10 mM Tris HCl (pH 8) and 5 mM $CaCl_2$. When required, OMVs were lysed by incubation with 1 % (vol/vol) Triton X-100 for 30 min at 37 °C. Intact and lysed OMVs were incubated for 60 min at 37 °C in the presence of 100 µg/ml proteinase K. The reaction was stopped by the addition of 5 mM phenylmethanesulfonyl fluoride (PMSF), and samples analyzed by SDS-PAGE and immunoblotting.

620

621 **MICs of OXA-23, CA_OXA-23, OXA-24 and CA_OXA-24**

622 To determine minimum inhibitory concentrations (MIC, µg/ml) of the β-lactam
623 antibiotics imipenem and piperacillin (Sigma-Aldrich®) on strains of *A. baumannii*
624 carrying OXAs we followed the standard agar plate protocol recommended by the
625 CLSI.

626

627 **Effect of OMVs loaded with OXAs on minimum inhibitory concentrations (MIC) of**
628 **bacteria**

629 To determine the minimum inhibitory concentrations (MIC, µg/ml) of the β-
630 lactam antibiotics imipenem and piperacillin (Sigma-Aldrich®) on β-lactam-susceptible
631 strains of *A. baumannii*, *E. coli*, and *P. aeruginosa* after treatment with OMVs, we
632 utilized OMVs purified from *A. baumannii* carrying an empty vector (EV) or expressing
633 either lipidated (OXA-23 or OXA-24/40) or soluble enzymes (CA_OXA-23 or CA_OXA-
634 24/40). We determined the MIC by broth-dilution method in 96-well plates according to
635 the CLSI guidelines. β-lactam-susceptible cells (5×10^5 CFU/ml) were inoculated into
636 medium without β-lactam or with 2-fold increasing concentrations of imipenem or
637 piperacillin, and with 1 µg/ml of OMVs from *A. baumannii* carrying an empty vector (EV)
638 or expressing OXAs. The 96-well plates were incubated at 37 °C with constant shaking
639 and the OD was recorded at 600 nm at 30 min time intervals, using a Biotek Epoch 2
640 microplate reader. MIC values were measured from two independent experiments.

641

642 **ACKNOWLEDGMENTS**

643 This research was supported by grants from the National Institutes of Health
644 (R01AI100560 to R.A.B. and A.J.V.), Agencia I+D+I (PICT-2020-00031 to A.J.V.),
645 MinCyT (REPARA to A.J.V.), the European Union's Horizon 2020 research and
646 innovation programme under the Marie Skłodowska-Curie (grant agreement No.
647 945363 to F.A.M.), and the Swiss National Science Foundation (CRSII5_198737 to

M.D.P.). A.J.V. and C.L. are staff members from CONICET. L.C. is recipient of fellowship from CONICET, Argentina. F.A.M. and M.D.P. are staff members of EPFL. We thank Marina Avecilla (IBR-CONICET) for her excellent technical assistance.

C.L. and A.J.V. designed research and supervised the study. L.C. and G.B. performed the bioinformatics analysis of the lipobox sequences. L.C. performed plasmid constructions for OXAs and their soluble variants, cell fractionation and protein localization, selective membrane solubilization and OXA immunodetection. C.L. performed OMVs purification, detection and determination of OXA levels into OMVs, proteinase K assay and protection assay with OMVs. F.A.M. performed the molecular simulation experiments. L.C., C.L. and F.A.M. designed the figures. All authors analyzed data, discussed results and contributed and edited manuscript. The content is solely the responsibility of the authors and does not necessarily represent the official views of the National Institutes of Health or the Department of Veterans Affairs.

REFERENCES

1. Bush K, Bradford PA. 2020. Epidemiology of β-lactamase-producing pathogens. *Clin Microbiol Rev* 33:00047-19.
2. Bonomo RA. 2017. β-Lactamases: a focus on current challenges. *Cold Spring Harb Perspect Med* 7:a025239.
3. Naas T, Oueslati S, Bonnin RA, Dabos ML, Zavala A, Dortet L, Retailleau P, Iorga BI. 2017. Beta-lactamase database (BLDB)–structure and function. *J Enzyme Inhib Med Chem* 32:917-919.
4. Llarrull LI, Testero SA, Fisher JF, Mobashery S. 2010. The future of the β-lactams. *Curr Opin Microbiol* 13:551-557.
5. Bush K, Jacoby GA. 2010. Updated functional classification of β-lactamases. *Antimicrob Agents Chemother* 54:969-976.
6. Tooke CL, Hinchliffe P, Bragginton EC, Colenso CK, Hirvonen VH, Takebayashi Y, Spencer J. 2019. β-Lactamases and β-Lactamase Inhibitors in the 21st Century. *J Mol Biol* 431:3472-3500.
7. Philippon A, Dusart J, Joris B, Frere J-M. 1998. The diversity, structure and regulation of β-lactamases. *Cell Mol Life Sci* 54:341-346.
8. Bahr G, Gonzalez LJ, Vila AJ. 2021. Metallo-β-lactamases in the age of multidrug resistance: from structure and mechanism to evolution, dissemination, and inhibitor design. *Chem Rev* 121:7957-8094.
9. Bonomo RA, Burd EM, Conly J, Limbago BM, Poirel L, Segre JA, Westblade LF. 2018. Carbapenemase-producing organisms: a global scourge. *Clin Infect Dis* 66:1290-1297.
10. McKenna M. 2013. The last resort: health officials are watching in horror as bacteria become resistant to powerful carbapenem antibiotics--one of the last drugs on the shelf. *Nature* 499:394-397.
11. Leonard DA, Bonomo RA, Powers RA. 2013. Class D β-lactamases: a reappraisal after five decades. *Acc Chem Res* 46:2407-2415.

690 12. Yoon E-J, Jeong SH. 2021. Class D β-lactamases. *J Antimicrob Chemother*
691 76:836-864.
692 13. Pradel N, Delmas J, Wu L, Santini C, Bonnet R. 2009. Sec-and Tat-dependent
693 translocation of β-lactamases across the Escherichia coli inner membrane.
694 *Antimicrob Agents Chemother* 53:242-248.
695 14. Denks K, Vogt A, Sachelaru I, Petriman N-A, Kudva R, Koch H-G. 2014. The
696 Sec translocon mediated protein transport in prokaryotes and eukaryotes. *Mol*
697 *Membr Biol* 31:58-84.
698 15. Morán-Barrio J, Limansky AS, Viale AM. 2009. Secretion of GOB metallo-β-
699 lactamase in Escherichia coli depends strictly on the cooperation between the
700 cytoplasmic DnaK chaperone system and the Sec machinery: completion of
701 folding and Zn (II) ion acquisition occur in the bacterial periplasm. *Antimicrob*
702 *Agents Chemother* 53:2908-2917.
703 16. Kaderabkova N, Bharathwaj M, Furniss RCD, Gonzalez D, Palmer T, Mavridou
704 DA. 2022. The biogenesis of β-lactamase enzymes. *Microbiol* 168:001217.
705 17. Bootsma HJ, van Dijk H, Verhoef J, Fleer A, Mooi FR. 1996. Molecular
706 characterization of the BRO beta-lactamase of Moraxella (Branhamella)
707 catarrhalis. *Antimicrob Agents Chemother* 40:966-972.
708 18. Randall LB, Dobos K, Papp-Wallace KM, Bonomo RA, Schweizer HP. 2016.
709 Membrane-bound PenA β-lactamase of Burkholderia pseudomallei. *Antimicrob*
710 *Agents Chemother* 60:1509-1514.
711 19. González LJ, Bahr G, Nakashige TG, Nolan EM, Bonomo RA, Vila AJ. 2016.
712 Membrane anchoring stabilizes and favors secretion of New Delhi metallo-β-
713 lactamase. *Nat chem bio* 12:516-522.
714 20. Martínez MM, Bonomo RA, Vila AJ, Maffía PC, González LJ. 2021. On the
715 offensive: the role of outer membrane vesicles in the successful dissemination
716 of New Delhi metallo-β-lactamase (NDM-1). Mbio 12:10.1128/mbio. 01836-21.

717 21. López C, Delmonti J, Bonomo RA, Vila AJ. 2022. Deciphering the evolution of
718 metallo-β-lactamases: A journey from the test tube to the bacterial periplasm. *J*
719 *Biol Chem* 298.
720 22. Auclair SM, Bhanu MK, Kendall DA. 2012. Signal peptidase I: cleaving the way
721 to mature proteins. *Protein Sci* 21:13-25.
722 23. Vogeley L, El Arnaout T, Bailey J, Stansfeld PJ, Boland C, Caffrey M. 2016.
723 Structural basis of lipoprotein signal peptidase II action and inhibition by the
724 antibiotic globomycin. *Science* 351:876-880.
725 24. Zückert WR. 2014. Secretion of bacterial lipoproteins: through the cytoplasmic
726 membrane, the periplasm and beyond. *Biochim Biophys Acta* 1843:1509-1516.
727 25. Narita S-i, Matsuyama S-i, Tokuda H. 2004. Lipoprotein trafficking in
728 Escherichia coli. *Arch Microbiol* 182:1-6.
729 26. Babu MM, Priya ML, Selvan AT, Madera M, Gough J, Aravind L, Sankaran K.
730 2006. A database of bacterial lipoproteins (DOLOP) with functional assignments
731 to predicted lipoproteins. *J bacteriol* 188:2761-2773.
732 27. Okuda S, Tokuda H. 2011. Lipoprotein sorting in bacteria. *Annu Rev Microbiol*
733 65:239-259.
734 28. Tanaka S-y, Narita S-i, Tokuda H. 2007. Characterization of the Pseudomonas
735 aeruginosa Lol system as a lipoprotein sorting mechanism. *J Biol Chem*
736 282:13379-13384.
737 29. Bei W, Luo Q, Shi H, Zhou H, Zhou M, Zhang X, Huang Y. 2022. Cryo-EM
738 structures of LolCDE reveal the molecular mechanism of bacterial lipoprotein
739 sorting in Escherichia coli. *PLoS Biol* 20:e3001823.
740 30. Toyofuku M, Nomura N, Eberl L. 2019. Types and origins of bacterial
741 membrane vesicles. *Nat Rev Microbiol* 17:13-24.
742 31. McBroom AJ, Kuehn MJ. 2005. Outer membrane vesicles. *EcoSal Plus*
743 1:10.1128/ecosal. 2.2. 4.

744 32. McMillan HM, Kuehn MJ. 2021. The extracellular vesicle generation paradox: a
745 bacterial point of view. *EMBO J* 40:e108174.
746 33. Brown L, Wolf JM, Prados-Rosales R, Casadevall A. 2015. Through the wall:
747 extracellular vesicles in Gram-positive bacteria, mycobacteria and fungi. *Nat*
748 *Rev Microb* 13:620-630.
749 34. Chatterjee S, Mondal A, Mitra S, Basu S. 2017. Acinetobacter baumannii
750 transfers the bla NDM-1 gene via outer membrane vesicles. *J Antimicrob*
751 *Chemother* 72:2201-2207.
752 35. Tang B, Yang A, Liu P, Wang Z, Jian Z, Chen X, Yan Q, Liang X, Liu W. 2023.
753 Outer Membrane Vesicles Transmitting bla NDM-1 Mediate the Emergence of
754 Carbapenem-Resistant Hypervirulent Klebsiella pneumoniae. *Antimicrob*
755 *Agents Chemother* 67:e01444-22.
756 36. Prunotto A, Bahr G, González LJ, Vila AJ, Dal Peraro M. 2020. Molecular bases
757 of the membrane association mechanism potentiating antibiotic resistance by
758 New Delhi metallo-β-lactamase 1. ACS infectious diseases 6:2719-2731.
759 37. López C, Prunotto A, Bahr G, Bonomo RA, González LJ, Dal Peraro M, Vila AJ.
760 2021. Specific protein-membrane interactions promote packaging of metallo-β-
761 lactamases into outer membrane vesicles. *Antimicrob Agents Chemother*
762 65:10.1128/aac. 00507-21.
763 38. Teufel F, Almagro Armenteros JJ, Johansen AR, Gíslason MH, Pihl SI, Tsirigos
764 KD, Winther O, Brunak S, von Heijne G, Nielsen H. 2022. SignalP 6.0 predicts
765 all five types of signal peptides using protein language models. *Nat Biotechnol*
766 40:1023-1025.
767 39. Hussain M, Pastor F, Lampen J. 1987. Cloning and sequencing of the blaZ
768 gene encoding beta-lactamase III, a lipoprotein of Bacillus cereus 569/H. *J*
769 *bacteriol* 169:579-586.
770 40. Souza PC, Alessandri R, Barnoud J, Thallmair S, Faustino I, Grünewald F,
771 Patmanidis I, Abdizadeh H, Bruininks BM, Wassenaar TA. 2021. Martini 3: a

772 general purpose force field for coarse-grained molecular dynamics. *Nat*
773 *methods* 18:382-388.
774 41. Abraham EP, Chain E. 1940. An enzyme from bacteria able to destroy
775 penicillin. *Nature* 146:837-837.
776 42. Hede K. 2014. Antibiotic resistance: An infectious arms race. *Nature* 509.
777 43. Lisa M-N, Palacios AR, Aitha M, González MM, Moreno DM, Crowder MW,
778 Bonomo RA, Spencer J, Tierney DL, Llarrull LI. 2017. A general reaction
779 mechanism for carbapenem hydrolysis by mononuclear and binuclear metallo-
780 β-lactamases. *Nat commun* 8:538.
781 44. Golemi D, Maveyraud L, Vakulenko S, Samama J-P, Mobashery S. 2001.
782 Critical involvement of a carbamylated lysine in catalytic function of class D β-
783 lactamases. *Proc Natl Acad Sci* 98:14280-14285.
784 45. Zhou Q, Catalán P, Bell H, Baumann P, Cooke R, Evans R, Yang J, Zhang Z,
785 Zappalà D, Zhang Y. 2023. An Ion-Pair Induced Intermediate Complex
786 Captured in Class D Carbapenemase Reveals Chloride Ion as a Janus Effector
787 Modulating Activity. *ACS Cent Sci* 9:2339-2349.
788 46. López C, Ayala JA, Bonomo RA, González LJ, Vila AJ. 2019. Protein
789 determinants of dissemination and host specificity of metallo-β-lactamases. *Nat*
790 *commun* 10:3617.
791 47. Bahr G, Vitor-Horen L, Bethel CR, Bonomo RA, González LJ, Vila AJ. 2018.
792 Clinical evolution of New Delhi metallo-β-lactamase (NDM) optimizes resistance
793 under Zn (II) deprivation. *Antimicrob Agents Chemother* 62:10.1128/aac.
794 01849-17.
795 48. Wu X, Chavez JD, Schweppe DK, Zheng C, Weisbrod CR, Eng JK, Murali A,
796 Lee SA, Ramage E, Gallagher LA. 2016. In vivo protein interaction network
797 analysis reveals porin-localized antibiotic inactivation in Acinetobacter
798 baumannii strain AB5075. *Nat Commun* 7:13414.

799 49. Yun SH, Park EC, Lee S-Y, Lee H, Choi C-W, Yi Y-S, Ro H-J, Lee JC, Jun S,
800 Kim H-Y. 2018. Antibiotic treatment modulates protein components of cytotoxic
801 outer membrane vesicles of multidrug-resistant clinical strain, Acinetobacter
802 baumannii DU202. *Clin Proteomics* 15:1-11.
803 50. Liao Y-T, Kuo S-C, Chiang M-H, Lee Y-T, Sung W-C, Chen Y-H, Chen T-L,
804 Fung C-P. 2015. Acinetobacter baumannii extracellular OXA-58 is primarily and
805 selectively released via outer membrane vesicles after Sec-dependent
806 periplasmic translocation. *Antimicrob Agents Chemother* 59:7346-7354.
807 51. Colquhoun JM, Farokhyfar M, Hutcheson AR, Anderson A, Bethel CR, Bonomo
808 RA, Clarke AJ, Rather PN. 2021. OXA-23 β-lactamase overexpression in
809 Acinetobacter baumannii drives physiological changes resulting in new genetic
810 vulnerabilities. *MBio* 12:e03137-21.
811 52. Marchaim D, Perez F, Lee J, Bheemreddy S, Hujer AM, Rudin S, Hayakawa K,
812 Lephart PR, Blunden C, Shango M. 2012. “Swimming in resistance”: co-
813 colonization with carbapenem-resistant Enterobacteriaceae and Acinetobacter
814 baumannii or Pseudomonas aeruginosa. *Am J infect Control* 40:830-835.
815 53. Maragakis LL, Tucker MG, Miller RG, Carroll KC, Perl TM. 2008. Incidence and
816 prevalence of multidrug-resistant Acinetobacter using targeted active
817 surveillance cultures. Jama 299:2513-2514.
818 54. Mammina C, Bonura C, Vivoli AR, Di Bernardo F, Sodano C, Saporito MA,
819 Verde MS, Saporito L, Cracchiolo AN, Fabbri PG. 2013. Co-colonization with
820 carbapenem-resistant Klebsiella pneumoniae and Acinetobacter baumannii in
821 intensive care unit patients. *Scand J Infec Dis* 45:629-634.
822 55. Semenec L, Cain AK, Dawson CJ, Liu Q, Dinh H, Lott H, Penesyan A,
823 Maharjan R, Short FL, Hassan KA. 2023. Cross-protection and cross-feeding
824 between Klebsiella pneumoniae and Acinetobacter baumannii promotes their
825 co-existence. *Nat Commun* 14:702.

826 56. Rumbo C, Fernández-Moreira E, Merino M, Poza M, Mendez JA, Soares NC,
827 Mosquera A, Chaves F, Bou G. 2011. Horizontal transfer of the OXA-24
828 carbapenemase gene via outer membrane vesicles: a new mechanism of
829 dissemination of carbapenem resistance genes in Acinetobacter baumannii.
830 *Antimicrob Agents Chemother* 55:3084-3090.
831 57. Cock PJ, Antao T, Chang JT, Chapman BA, Cox CJ, Dalke A, Friedberg I,
832 Hamelryck T, Kauff F, Wilczynski B. 2009. Biopython: freely available Python
833 tools for computational molecular biology and bioinformatics. *Bioinform*
834 25:1422.
835 58. Varadi M, Anyango S, Deshpande M, Nair S, Natassia C, Yordanova G, Yuan
836 D, Stroe O, Wood G, Laydon A. 2022. AlphaFold Protein Structure Database:
837 massively expanding the structural coverage of protein-sequence space with
838 high-accuracy models. Nucleic Acids Res 50:D439-D444.
839 59. Ruch P, Teodoro D, Consortium U. 2021. Uniprot.
840 60. Berman HM, Westbrook J, Feng Z, Gilliland G, Bhat TN, Weissig H, Shindyalov
841 IN, Bourne PE. 2000. The protein data bank. *Nucleic Acids Res* 28:235-242.
842 61. Kroon PC, Grünewald F, Barnoud J, van Tilburg M, Souza PC, Wassenaar TA,
843 Marrink S-J. 2022. Martinize2 and vermouth: Unified framework for topology
844 generation. arXiv preprint arXiv:221201191.
845 62. Rao S, Bates GT, Matthews CR, Newport TD, Vickery ON, Stansfeld PJ. 2020.
846 Characterizing membrane association and periplasmic transfer of bacterial
847 lipoproteins through molecular dynamics simulations. *Struct* 28:475-487. e3.
848 63. Wassenaar TA, Ingólfsson HI, Bockmann RA, Tieleman DP, Marrink SJ. 2015.
849 Computational lipidomics with insane: a versatile tool for generating custom
850 membranes for molecular simulations. *J Chemical Theory Comput* 11:2144-
851 2155.
852 64. Jiang X, Yang K, Yuan B, Han M, Zhu Y, Roberts KD, Patil NA, Li J, Gong B,
853 Hancock RE. 2020. Molecular dynamics simulations informed by membrane

854 lipidomics reveal the structure–interaction relationship of polymyxins with the
855 lipid A-based outer membrane of Acinetobacter baumannii. *J Antimicrob*
856 *Chemother* 75:3534-3543.
857 65. Corey RA, Song W, Duncan AL, Ansell TB, Sansom MS, Stansfeld PJ. 2021.
858 Identification and assessment of cardiolipin interactions with E. coli inner
859 membrane proteins. *Sci adv* 7:eabh2217.
860 66. Abraham MJ, Murtola T, Schulz R, Páll S, Smith JC, Hess B, Lindahl E. 2015.
861 GROMACS: High performance molecular simulations through multi-level
862 parallelism from laptops to supercomputers. SoftwareX 1:19-25.
863 67. Tironi IG, Sperb R, Smith PE, van Gunsteren WF. 1995. A generalized reaction
864 field method for molecular dynamics simulations. *J Chem Phys* 102:5451-5459.
865 68. Jo S, Kim T, Iyer VG, Im W. 2008. CHARMM-GUI: a web-based graphical user
866 interface for CHARMM. J Comp Chem 29:1859-1865.
867 69. Bussi G, Donadio D, Parrinello M. 2007. Canonical sampling through velocity
868 rescaling. *J Chem Phys* 126.
869 70. Parrinello M, Rahman A. 1980. Crystal structure and pair potentials: A
870 molecular-dynamics study. Phys Rev Lett 45:1196.
871 71. Sejdiu BI, Tieleman DP. 2021. ProLint: a web-based framework for the
872 automated data analysis and visualization of lipid–protein interactions. *Nucleic*
873 *Acids Res* 49:W544-W550.
874 72. Humphrey W, Dalke A, Schulten K. 1996. VMD: visual molecular dynamics. *J*
875 *Mol Graph* 14:33-38.
876 73. Goddard TD, Huang CC, Meng EC, Pettersen EF, Couch GS, Morris JH, Ferrin
877 TE. 2018. UCSF ChimeraX: Meeting modern challenges in visualization and
878 analysis. Prot Sci 27:14-25.
879 74. Petiti M, Houot L, Duché D. 2017. Cell fractionation. *Methods Mol Biol*:59-64.
880 75. GelAnalyzer 23.1.1 (available at www.gelanalyzer.com) by Istvan Lazar Jr.,
881 PhD and Istvan Lazar Sr., PhD, CSc

882 76. Schwechheimer C, Kulp A, Kuehn MJ. 2014. Modulation of bacterial outer
883 membrane vesicle production by envelope structure and content. *BMC*
884 *Microbiol* 14:1-13.
885
886

887 **FIGURE LEGENDS**

888 **Fig 1. Class D contains the largest family of putative lipidated β-lactamases. (A)**
889 Pie chart indicating the number of β-lactamase sequences predicted to be translocated
890 by the Sec and Tat systems. The bar at the right shows the distribution of β-lactamases
891 translocated by the Tat system in each class, detailing if they are putative substrates of
892 SpI (putative soluble proteins) or SpII (putative lipoproteins). **(B)** Putative substrates of
893 SpI or SpII translocated by the Sec system, separated according to the β-lactamase
894 class. The absolute numbers of each category are indicated inside each bar. The three
895 subclasses of class B enzymes (B1, B2 and B3) are indicated at the right. Class D
896 enzymes show the largest number of predicted lipoproteins.
897
898 **Fig 2. Residue-wise contact frequency (%) with cardiolipin lipids during the**
899 **simulations.** (A) OXA-23 and OXA-24/40 contact frequency (measured as percentage
900 of simulation time) with cardiolipin, color coded from white (0% frequency) to red
901 (85.5% frequency). The lipidated cysteines (Cys18 and Cys20) are indicated in the N-
902 terminus of both β-lactamases. Active site residues are shown as spheres. (B) A close-
903 up of the residues (shown as sticks) on the opposite side of the active-site (shown as
904 spheres). These positively charged residues also contribute to membrane binding,
905 positioning the active-site towards the periplasm and preventing its occlusion.
906
907 **Fig 3. OXA-23 and OXA-24/40 are membrane anchored proteins while OXA-48 is**
908 **soluble periplasmic.** (A) N-terminal sequences of the OXAs object of the experimental
909 analysis. The lipoboxes are underlined and the cysteine target of lipidation is bolded.
910 (B) Cell fractionation of *A. baumannii* ATCC 17978 expressing OXA-23 and OXA-
911 24/40, and *E. coli* ATCC 25922 expressing OXA-48 (C) Cell fractionation of *A.*
912 *baumannii* expressing the Cys18Ala-OXA-23 (CA_OXA-23) and Cys20Ala-OXA-24/40
913 (CA_OXA-24/40) variants. (D) Solubilization assays of OXA-23 and OXA-24/40 from *A.*
914 *baumannii* total membranes. OXA-ST indicates the bands corresponding to anti-ST

915 antibodies, which match with the molecular weight of the enzymes fused to the tag.
916 OmpA indicated the bands revealed by anti-OmpA antibodies which recognize the
917 outer membrane protein OmpA. RNApol indicated the bands revealed using RNA
918 polymerase antibodies.
919
920 **Fig 4. Membrane anchored OXAs are incorporated in higher proportions into**
921 **OMVs than periplasmic soluble OXAs.** (A) Anti-ST immunoblotting of whole cells
922 (WC) and outer membrane vesicles (OMVs) from *A. baumannii* ATCC 17978
923 expressing OXA-23 or OXA-24/40 and its soluble variants (CA_OXA-23 or CA_OXA-
924 24/40). (B) Comparison between the percentages (%) of the levels of the soluble
925 variants CA_OXA-23 and CA_OXA-24/40 into OMVs. The plotted values, normalized to
926 the corresponding wild-type OXA (lipidated OXA) levels, were obtained as described in
927 Materials and Methods. Data correspond to three independent experiments (black filled
928 symbols) and are shown as the mean value. Error bars represent standard deviations
929 (SD). P-values according to the Student's t-test: **p ≤ 0.01, ***p ≤ 0.001. (C) Anti-ST
930 immunoblotting of OMVs from *A. baumannii* carrying OXA-23 or OXA-24/40 treated
931 with and without Proteinase K and 1% v/v Triton X-100.
932
933 **Fig 5. OMVs loaded with lipidated OXAs provide enhanced protection to β-**
934 **lactam-susceptible bacteria than OMVs containing soluble variants.** MIC values
935 (μg/ml) against (A) imipenem and (B) piperacillin of β-lactam susceptible *A. baumannii*,
936 *E. coli* and *P. aeruginosa* cells after treatment with OMVs purified from *A. baumannii*
937 carrying empty the vector (EV) or expressing lipidated enzymes: OXA-23 or OXA-24/40
938 or soluble enzymes: CA_OXA-23 or CA_OXA-24/40. Data correspond to mean values
939 from two independent experiments. Error bars represent standard deviations (SD). The
940 MICs of susceptible bacteria against imipenem or piperacillin (without incubation with
941 OMVs) are shown in Supplementary Table 3.

942 **Table 1. β-lactamases from classes A and B with lipoboxes in their signal**
943 **peptides.** The asterisk next to the lactamase names indicate the enzymes for which
944 the membrane localization has been experimentally assessed. The most frequent
945 organisms expressing the lactamase gene are indicated in the third column.

Ambler class or subclass	β-lactamase	Organism	Translocation system
A	BcIII*	*Bacillus cereus*	Sec/SpII
A	BlaC	*Mycobacterium tuberculosis*	Tat/SpII
A	BlaP-1/2	*Bacillus licheniformis*	Sec/SpII
A	BRO-1*/2*	*Moraxella catarrhalis*	Tat/SpII
A	PC-1*	*Staphylococcus aureus*	Sec/SpII
A	PenA-1/39	*Burkholderia multivorans*	Tat/SpII
A	PenI-1/8*	*Burkholderia pseudomallei*	Tat/SpII
A	ROB-1/5, 8/13	*Pasteurellales, Moraxella spp.*	Sec/SpII
B1	AFM-1/4	*Burkholderiales, Pseudomonas spp.*	Sec/SpII
B1	NDM-1/68*	Enterobacterales, non-fermenters	Sec/SpII
B3	ECM-1	*Erythrobacter citreus*	Sec/SpII
B3	EFM-1	*Erythrobacter flavus*	Sec/SpII
B3	EVM-1	*Erythrobacter vulgaris*	Sec/SpII

946

947 **Table 2. Predicted cellular localization of principal class D β-lactamases.** In the
948 organism column are specified the most reported organism carrying the lactamase
949 gene or the order they belong to. The three OXA proteins selected in this study are
950 highlighted in red (OXA-23, 24/40 and 48, the representative members of each of these
951 families). Supplementary Table 2 describes all OXA-subfamilies.
952

Class D β-lactamase	Number of enzymes	Organism(s)	Predicted cell localization
OXA-1-like	12	*Pseudomonadales, Shewanellaceae, Pasteurellales, Enterobacterales*	soluble
OXA-2-like	31	*Pseudomonadales, Burkholderiales, Shewanellaceae, Enterobacterales, Vibrionales, Pasteurellales*	soluble
OXA-10-like	60	*Burkholderiales, Pseudomonadales, Shewanellaceae, Enterobacterales*	soluble
OXA-22-like	7	*Ralstonia* spp.	soluble
OXA-23-like	49	*Acinetobacter* spp. *	lipidated
OXA-24/40-like	24	*Acinetobacter* spp.	lipidated
OXA-48-like	66	Enterobacterales, Shewanellaceae	soluble
OXA-50-like	60	*Pseudomonas* spp.	soluble
OXA-51-like	382	*Acinetobacter* spp.	lipidated
OXA-58-like	8	*Acinetobacter* spp.	lipidated
OXA-60-like	7	*Ralstonia* spp.	soluble
OXA-134-like	34	*Acinetobacter* spp.	lipidated
OXA-61-like	49	*Campylobacter* spp.	soluble
OXA-211-like	17	*Acinetobacter* spp.	lipidated
OXA-213-like	51	*Acinetobacter* spp.	lipidated

953

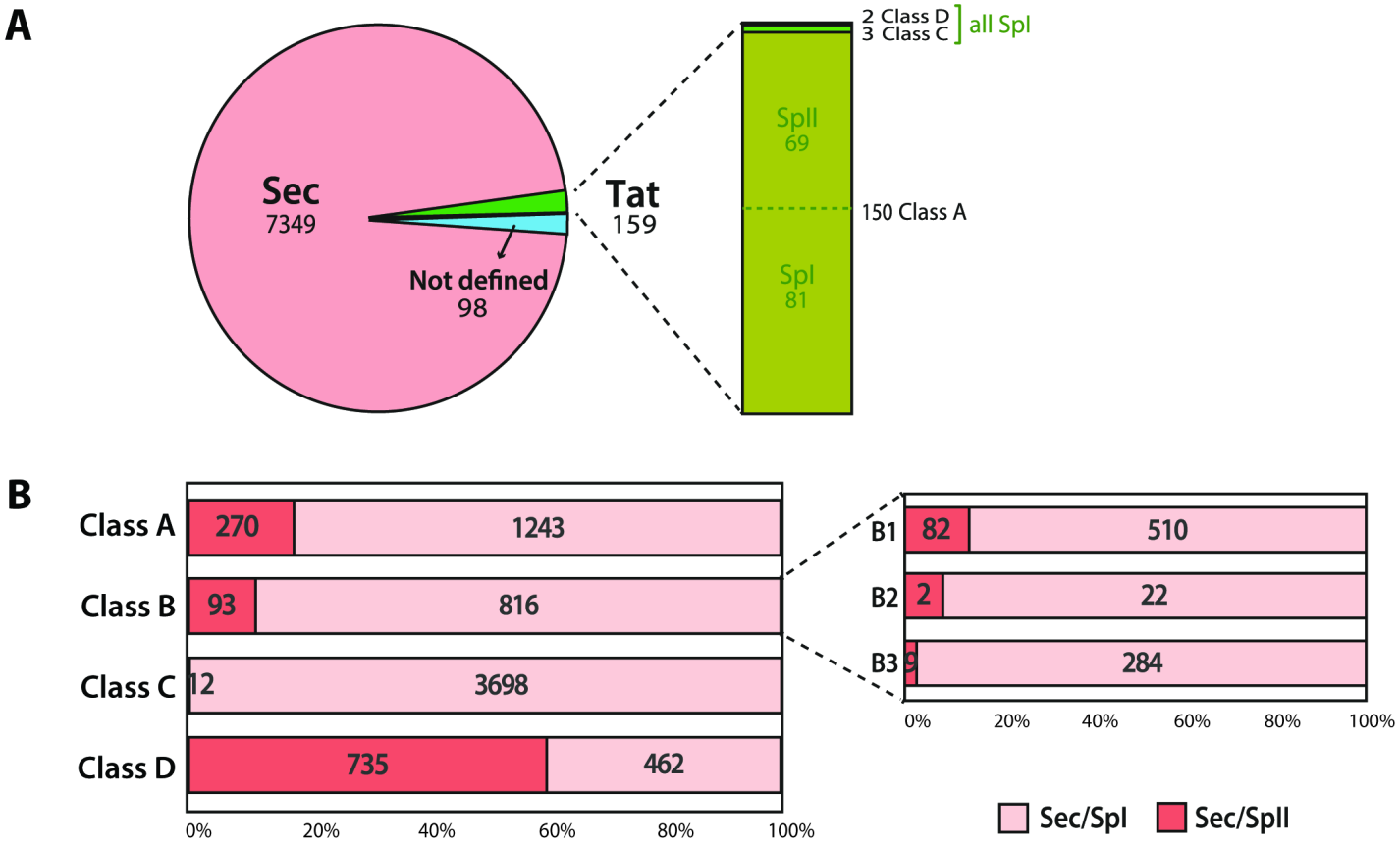
A
Sec
7349
Not defined
98
Tat
159
SpII
69
Spl
81
2 Class D
3 Class C
all Spl
150 Class A
B
Class A
Class B
Class C
Class D
270
1243
93
816
12
3698
735
462
0%
20%
40%
60%
80%
100%
B1
B2
B3
82
510
2
22
9
284
Sec/Spl
Sec/SpII

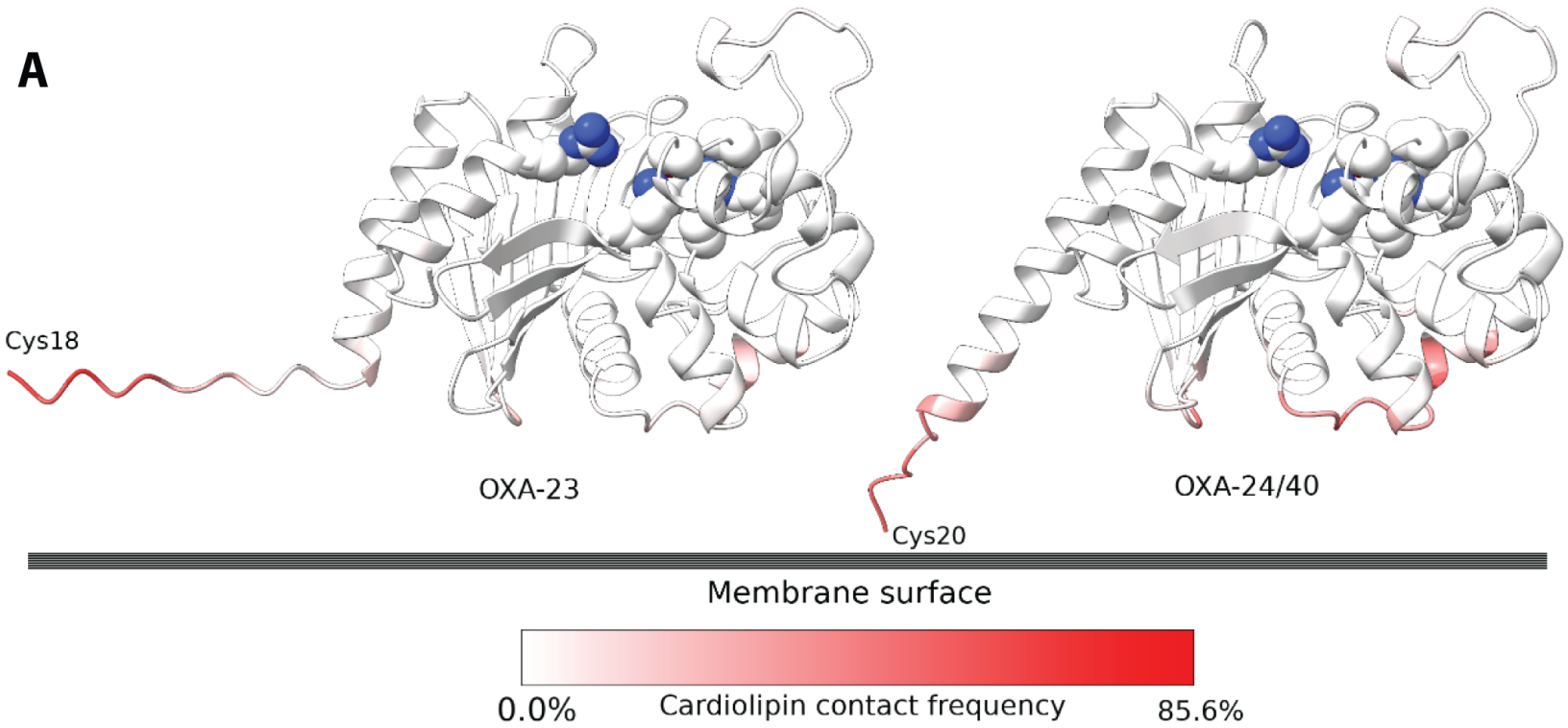
A
Cys18
OXA-23
OXA-24/40
Cys20
Membrane surface
0.0%
Cardiolipin contact frequency
85.6%

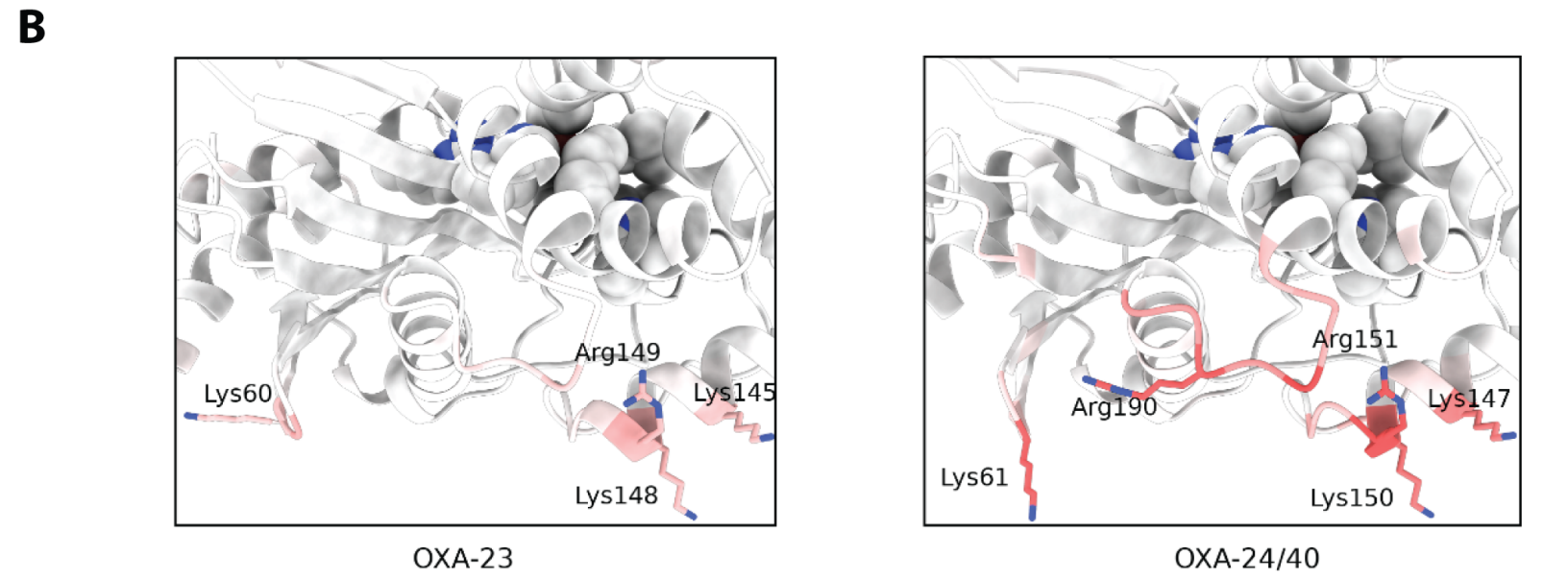
B
Arg149
Lys60
Lys145
Lys148
OXA-23
Arg151
Arg190
Lys147
Lys61
Lys150
OXA-24/40

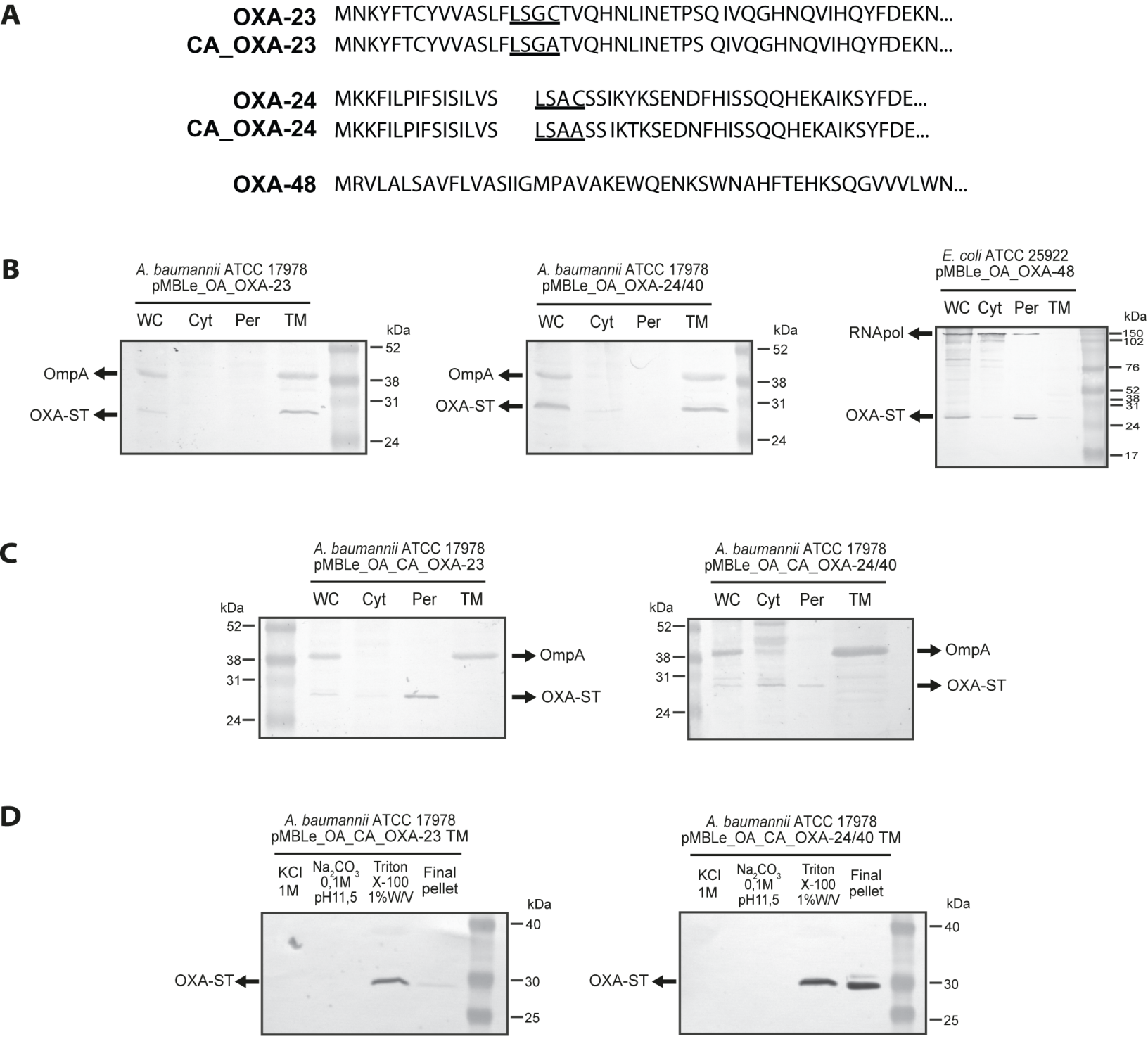
A
OXA-23 MNKYFTCYVVASLFLSGCTVQHNLINETPSQ IVQGHNQVIHQYFDEKN...
CA_OXA-23 MNKYFTCYVVASLFLSGATVQHNLINETPS QIVQGHNQVIHQYFDEKN...
OXA-24 MKKFILPIFSISILVS LSACSSIKYKSENDFHISSQQHEKAIKSYFDE...
CA_OXA-24 MKKFILPIFSISILVS LSAASS IKTKSEDNFHISSQQHEKAIKSYFDE...
OXA-48 MRVLALSAVFLVASIIGMPAVAKEWQENKSWNAHFTEHKSQGVVVLWN...
B
A. baumannii ATCC 17978 pMBLe_OA_OXA-23
WC Cyt Per TM
kDa
52
38
31
24
OmpA
OXA-ST
A. baumannii ATCC 17978 pMBLe_OA_OXA-24/40
WC Cyt Per TM
kDa
52
38
31
24
OmpA
OXA-ST
E. coli ATCC 25922 pMBLe_OA_OXA-48
WC Cyt Per TM
kDa
150
102
76
52
38
31
24
17
RNApol
OXA-ST
C
A. baumannii ATCC 17978 pMBLe_OA_CA_OXA-23
WC Cyt Per TM
kDa
52
38
31
24
OmpA
OXA-ST
A. baumannii ATCC 17978 pMBLe_OA_CA_OXA-24/40
WC Cyt Per TM
kDa
52
38
31
24
OmpA
OXA-ST
D
A. baumannii ATCC 17978 pMBLe_OA_CA_OXA-23 TM
KCl 1M
Na2CO3 0,1M pH11,5
Triton X-100 1%W/V
Final pellet
kDa
40
30
25
OXA-ST
A. baumannii ATCC 17978 pMBLe_OA_CA_OXA-24/40 TM
KCl 1M
Na2CO3 0,1M pH11,5
Triton X-100 1%W/V
Final pellet
kDa
40
30
25
OXA-ST

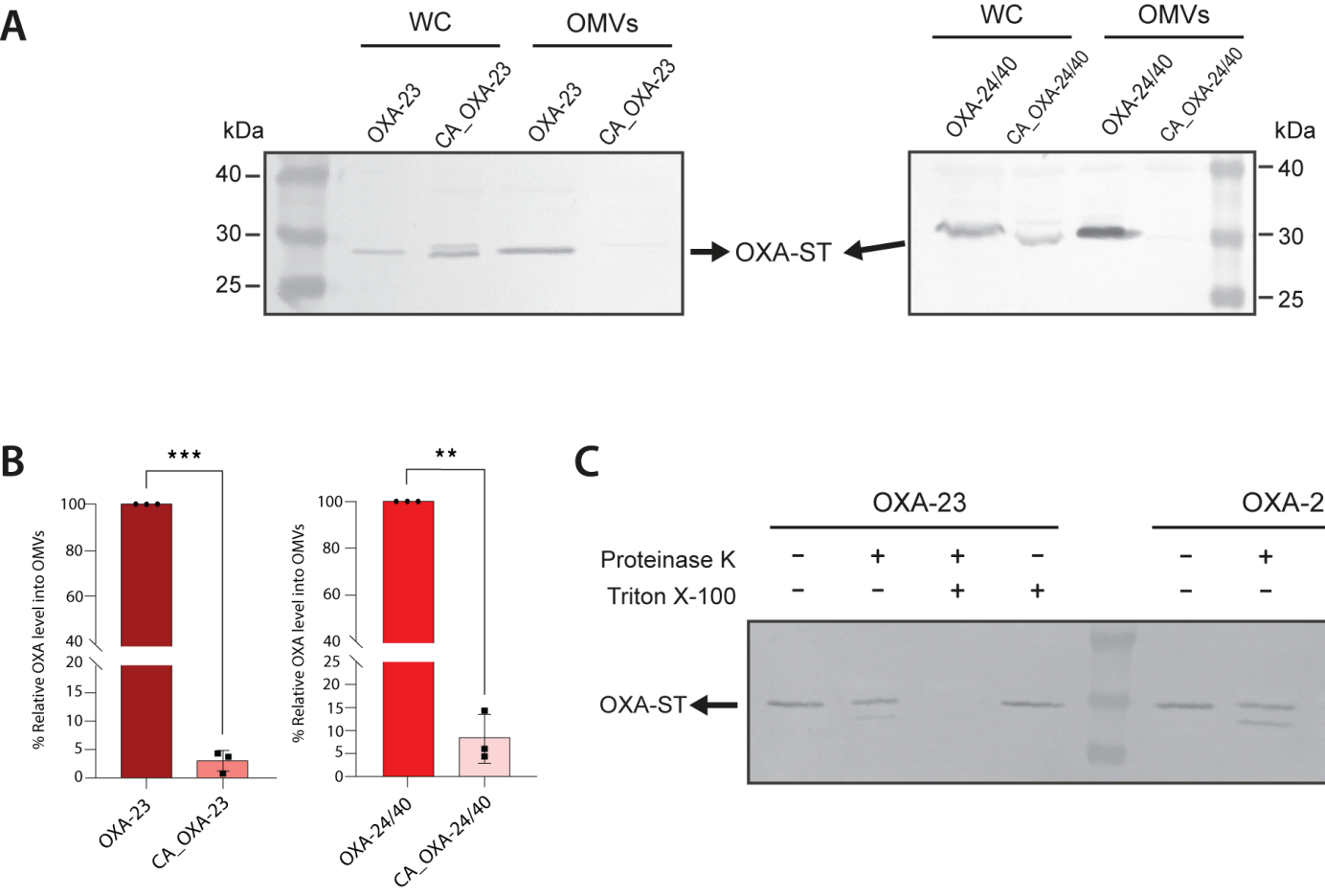
A
WC
OMVs
WC
OMVs
kDa
OXA-23
CA_OXA-23
OXA-23
CA_OXA-23
OXA-24/40
CA_OXA-24/40
OXA-24/40
CA_OXA-24/40
kDa
40
30
25
OXA-ST
40
30
25
B
***
**
% Relative OXA level into OMVs
100
80
60
40
20
15
10
5
0
25
OXA-23
CA_OXA-23
OXA-24/40
CA_OXA-24/40
C
OXA-23
OXA-24/40
Proteinase K
Triton X-100
kDa
OXA-ST
40
30
25

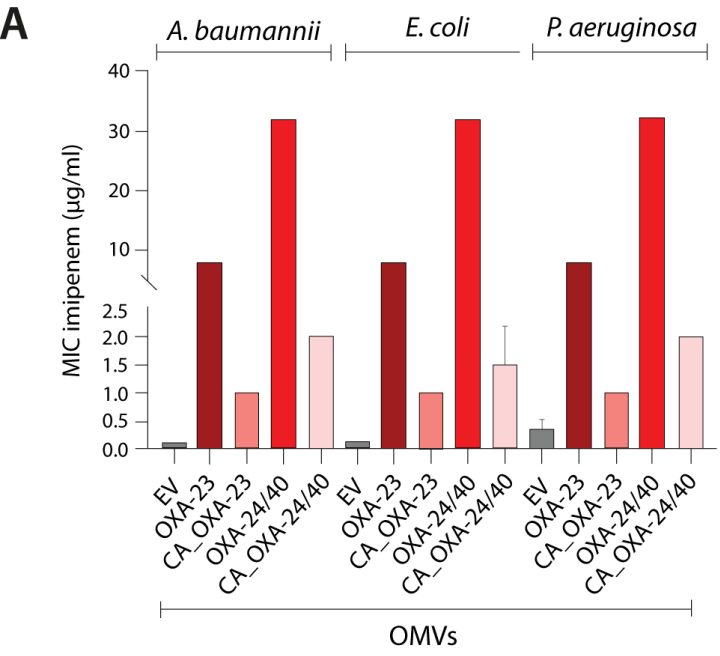
A
A. baumannii
E. coli
P. aeruginosa
MIC imipenem (µg/ml)
40
30
20
10
2.5
2.0
1.5
1.0
0.5
0.0
EV
OXA-23
CA_OXA-23
OXA-24/40
CA_OXA-24/40
OMVs

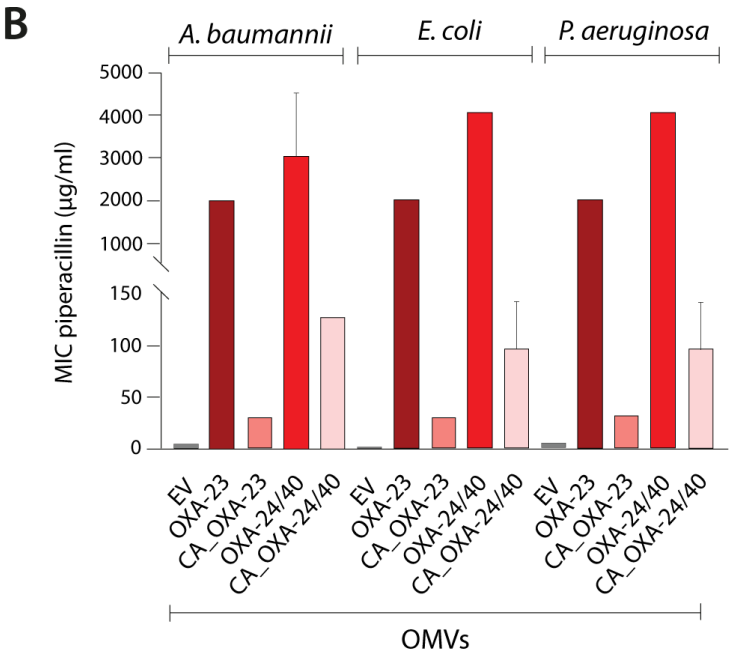
B
A. baumannii
E. coli
P. aeruginosa
MIC piperacillin (µg/ml)
5000
4000
3000
2000
1000
150
100
50
0
EV
OXA-23
CA_OXA-23
OXA-24/40
CA_OXA-24/40
OMVs